Tap Reactor for Temporally and Spatially Resolved Analysis of the CO_2 Methanation Reaction

Timo Engl, Moritz Langer, Hannsjörg Freund, Michael Rubin*, and Roland Dittmeyer

DOI: 10.1002/cite.202200204

This is an open access article under the terms of the Creative Commons Attribution-NonCommercial-NoDerivs License, which permits use and distribution in any medium, provided the original work is properly cited, the use is non-commercial and no modifications or adaptations are made.

Supporting Information available online

Chemical energy carriers produced according to power-to-X concepts will play a crucial role in the future energy system. Here, CO_2 methanation is described as one promising route. However, transient operating conditions and the resulting effects on catalyst stability are to be considered. In this contribution, a tap reactor for spatially and temporally resolved analysis of the methanation reaction is presented. The Ni catalyst investigated was implemented as coating. Reaction data as a function of time and reactor coordinate under various operating conditions are presented and discussed. A comparison with simulation data validates the presented tap reactor concept.

Keywords: Catalyst coatings, CO_2 methanation, Spatially and temporally resolved analysis, Tap reactors, Transient operation

Received: November 15, 2022; *revised:* January 23, 2023; *accepted:* February 23, 2023

1 Introduction

To limit the effects of the climate crisis mankind is facing, and recently also due to political instabilities, society and industry is in urgent need for renewable alternatives to the currently used fossil sources for fuels, power generation, and feedstock for the chemical process industries [1]. To tackle the challenge of an independent and renewable energy economy, fossil fuels have to be substituted by green chemical energy carriers where direct electrification is not (yet) possible. One piece of the puzzle of a future green energy system will be power-to-X (PtX) processes. In the context of replacing conventional fossil fuels, the "X" in PtX represents hydrocarbons which can provide CO_2-neutral chemical energy carriers, i.e., high energy molecules such as methane, liquid hydrocarbons, or oxygenates, when green electricity for electrolysis ("Power-to") and non-fossil carbon sources are used. In the last decade, methanation received increased attention since methane is already used by various industries and can easily be distributed using the existing natural gas grids.

The catalytic hydrogenation of CO_2 first discovered by Sabatier in 1902 [2, 3] is a highly exothermal reaction influenced by the thermal dynamic equilibrium and volume reduction as given in Eq. (1). Baraj et al. [4] state two different reaction routes, either by direct methanation or through the formation of CO via the reverse water-gas shift (rWGS) reaction (Eq. (2)) with subsequent CO hydrogenation (Eq. (3)).

$$CO_2 + 4H_2 \rightleftharpoons CH_4 + 2H_2O \quad \Delta H_R^0 = -165\ \text{kJ mol}^{-1} \tag{1}$$

$$CO_2 + H_2 \rightleftharpoons CO + H_2O \quad \Delta H_R^0 = 41\ \text{kJ mol}^{-1} \tag{2}$$

$$CO + 3H_2 \rightleftharpoons CH_4 + H_2O \quad \Delta H_R^0 = -206\ \text{kJ mol}^{-1} \tag{3}$$

The major challenge of any PtX process is its fluctuating availability and limited quantity of green electricity at the very site of power generation. Thus, the usage of decentralized and dynamically operated process chains (power generation – electrolysis – synthesis) is favorable, especially when larger buffer tanks for H_2 and/or CO_2 are to be avoided.

[1]Timo Engl, [2]Moritz Langer, [2]Prof. Dr.-Ing. Hannsjörg Freund, [1,3]Dr.-Ing. Michael Rubin
https://orcid.org/0000-0002-2670-0887
(michael.rubin@kit.edu),
[1,3]Prof. Dr.-Ing. Roland Dittmeyer
https://orcid.org/0000-0002-3110-6989

[1]Karlsruhe Institute of Technology, Institute for Micro Process Engineering (IMVT), Hermann-von-Helmholtz-Platz 1, 76344 Eggenstein-Leopoldshafen, Germany.

[2]TU Dortmund University, Institute of Reaction Engineering and Catalysis (REC), Emil-Figge-Straße 66, 44227 Dortmund, Germany.

[3]Karlsruhe Institute of Technology, Institute of Catalysis Research and Technology (IKFT), Hermann-von-Helmholtz-Platz 1, 76344 Eggenstein-Leopoldshafen, Germany.

 © 2023 The Authors. Chemie Ingenieur Technik published by Wiley-VCH GmbH

This, however, requires a deeper understanding of the capability to be operated under non-stationary conditions of both, process technology and catalysts involved [5].

The field of dynamic operated methanation has received increasing interest [6–8]. However, there are only a few studies published which investigated dynamically operated methanation [9–12] with special focus on fluctuating feed flows and their influence on catalyst activity and stability. In particular, the oxidation of the Ni particles during H_2 dropout scenarios (removal of H_2 from the feed) resulted in a lower catalytic performance in the subsequent methanation step. To obtain a deeper insight into the dynamically operated reaction and its kinetics, spatially resolved reactors gather valuable data about the reaction progress. In the past years, several spatially resolved reactor types, e.g., monolith [13–17], catalytic foam [18–20], and catalytic plate [21–25] reactors, have been developed and applied in research. All reactors work according to the same principle: a sampling capillary is moved lengthwise through the reactor gathering gas samples on various positions. Due to the moving capillary, especially in fixed-bed reactors an influence on the structure of the catalytic bed cannot be avoided and an accurate mass distribution along the reactor length can hardly be determined. However, in the case of the catalytic plate reactor, computational fluid dynamics simulations have shown that the influence of the capillary is only marginal [25].

Aiming to get a deeper insight into the methanation reaction also under transient operating conditions, this contribution presents a tap reactor with five consecutive reaction zones (RZs) each with a specific catalyst mass. This reactor allows the sampling of gas phase compositions between the RZs via four taps leading to a spatially resolved concentration profile along the reactor. The basic design of the reactor, the concept and realization of the catalyst integration as well as exemplary results of transient operation are presented. Besides, the data obtained experimentally are compared with simulation data obtained using a plug-flow reactor model.

2 Materials and Methods

2.1 Tap Reactor with Coated Catalyst on Microstructured Foils

To allow for spatially and temporally resolved analysis of the gas phase composition, a tap reactor (Fig. 1a), which was designed and built in-house, was used in the investigations. As depicted in Fig. 1b, the reaction chamber is a flat channel (22 mm × 143 mm, depth 1 mm) inside the reactor body (Nicrofer®, 1.4876). It consists of five deepenings (24 mm × 24 mm, depth 40 µm), representing the five reaction zones where the microstructured foils coated with the catalyst can be placed. Between each RZ there is a space of 2 mm with a borehole allowing for gas sampling via a capillary (0.8 mm inner diameter) welded to the bottom of the reactor body. The capillaries connect the accordant sampling position with the multiport valve of the GC (six individual storage loops), thus allowing spatially resolved gas sampling. The sealing of the reaction chamber is achieved by a graphite sealing which is pressed between the reactor lid and the bottom part. The actual reactor body is merged with a copper plate containing seven individually controlled electrical heating cartridges (inlet, outlet, five directly underneath each RZ) allowing for a homogeneous and isothermal temperature profile (measured by eight thermocouples directly underneath the RZs) along the reaction coordinate. Isothermal conditions can be assumed as the heat of reaction is negligible in comparison to the heating power needed to maintain the setpoint temperature in the given reactor system when running the reaction. The reactants are fed through a slit from below the reaction chamber and guided over the catalytic layers before leaving the reactor likewise through a slit. The tap reactor is designed for a maximum temperature of T_R = 450 °C and a maximum pressure of p_R = 20 bar, which is in the range of the industrial methanation reaction and insulated against heat loss using isoplan 1000® material.

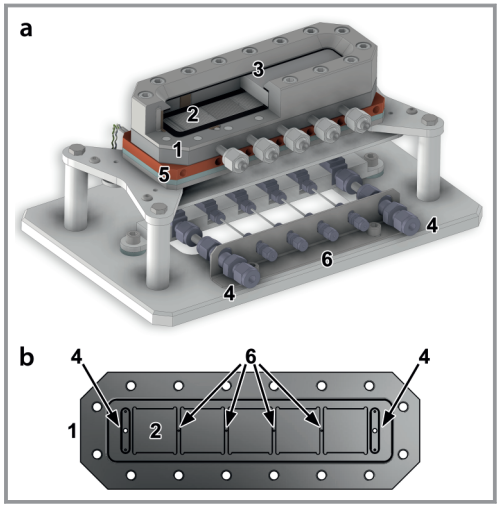

Figure 1. a) Schematic representation of the methanation tap reactor and b) details of the reaction chamber. (1) Reaction chamber with five reaction zones for hosting the five microstructured foils (2) coated with the catalyst, (3) reactor body and lid, (4) inlet and outlet connections, (5) copper base plate including seven heating cartridges to ensure homogeneous heat distribution, (6) capillaries for gathering spatially resolved gas samples in between the individual reaction zones.

2.2 Catalyst Layer Preparation via Screen Printing

In this study, an industrial Ni/Al_2O_3 methanation reference catalyst (denoted as SPP2080-IMRC; IMRC = industrial methanation reference catalyst) was used. Various studies were performed in the recent years [26–28] which focused on the investigation of the structure, morphology, and activ-

 © 2023 The Authors. Chemie Ingenieur Technik published by Wiley-VCH GmbH

15222640, 0, Downloaded from https://onlinelibrary.wiley.com/doi/10.1002/cite.202200204 by Karlsruher Inst F. Technologie, Wiley Online Library on [16/04/2023]. See the Terms and Conditions (https://onlinelibrary.wiley.com/terms-and-conditions) on Wiley Online Library for rules of use; OA articles are governed by the applicable Creative Commons License

ity of the catalyst in the frame of the priority program 2080 funded by the German Research Foundation (DFG). Weber et al. [27] determined the nickel amount of 8.6 wt % with traces of iron of 0.01 wt %. The authors further investigated the reduction temperature via (H_2-temperature programmed reduction) and found that the NiO reduction to Ni^0 peaks at approx. 270 °C. One key feature of the tap reactor presented in the present study is the catalyst implementation in form of a layer forming independent catalyst, i.e., reaction zones within the reactor. The tap reactor is built to contain five microstructured foils (see Sect. 2.1) which need to be coated with the catalyst – therefore, screen printing was applied. In the first step, the SPP2080-IMR-catalyst spheres (2.5 mm diameter) were ground to obtain a fine powder, which is required for the paste preparation. In particular, the catalyst was ground twice using a ball mill (wet milling with isopropanol, jar and balls out of ZrO_2 to ensure a low amount of abrasion) to obtain a catalyst particle size smaller than 3 µm.

To achieve homogeneous and reproducible layers via screen printing, the catalyst paste has to meet certain rheologic characteristics. In preliminary studies, the paste recipe was optimized in terms of final paste rheology and applied in the present work (Tab. 1). The solvent (terpineol, Thermo Fisher), thickener (ethyl cellulose, Aldrich Chemistry), and dispersant (Hypermer KD1, Croda Europe Ltd) were mixed and stirred (magnetic stirrer) at 300 rpm for 15 min at 60 °C in a beaker heated by a water bath before the catalyst powder was added to the solution and further stirred for 15 min under the same conditions. After cooling to room temperature, the resulting paste was further homogenized using a three-roll mill (Exakt, 50i) and stored in a fridge at 3 °C for further use in screen printing.

Table 1. Composition of the pastes prepared for screen printing.

Component	Fraction [wt %]
Catalyst	35
Terpineol	59.2
Ethyl cellulose	0.4
Hypermer KD1	5.4

In Fig. S1 in the Supporting Information, the microstructured foil (stainless steel 1.4876), serving as the substrate for the catalyst layers, is shown. Each plate (24 × 24 mm) contains 15 etched channels of approx. 40 µm in depth and 1.24 mm in width. Before the actual coating, the foils were heat-treated for 1 h at 800 °C (6 K min^{-1}) in air to clean the surface and create an oxide layer being beneficial for adherence of the layer to be coated. Printing was conducted using a semi-automated screen printer (EKRA E2). The coated foils were dried for approx. 2 h at 60 °C in a drying oven with subsequent heat treatment for 1 h at 200 °C (2 K min^{-1}) in a calcination oven to remove the suspending agent terpineol and increase adherence. The resulting layers were characterized by means of SEM imaging (Jeol JSM-6300) and profilometry (Sensofar SNeox in confocal mode) to quantify the layer thickness achieved and qualitatively evaluate the layer morphology.

2.3 Test Rig and Operating Conditions

The tap reactor was operated within a test rig consisting of gas supply via mass flow, pressure and temperature controllers. The feed gases (CO_2 and H_2, N_2 for dilution and internal standard) are mixed and preheated to 180 °C before being fed into the tap reactor. As outlined in Sect. 2.1, the reactants pass five different reaction zones (RZ1 to RZ5) each of which contains a catalyst-coated microstructured foil (see Sect. 2.2). Between every RZ as well as at the inlet and outlet of the reactor there is a tap allowing for sampling the gas composition at the very position of the reactor coordinate. To allow for spatially (reactor coordinate = variable, time on stream (*TOS*) = const.) or temporally (reactor coordinate = const., *TOS* = variable) resolved analysis, the gas chromatograph (GC 8860, Agilent) is equipped with six storage loops (capillaries, volume of 2 ml each). The configuration of the GC is designed to analyze CH_4, CO_2, H_2, N_2, and CO. The samples in the loaded storage loops can then be analyzed successively via the GC. With the tap system, a set of six gas samples with a temporal resolution of 11 s (limited by sufficient flushing of the sample loops) can be gathered every 120 min (limited by the duration of the actual GC measurement). To assure a sufficiently pure gas sample, in between measurements the storage loops are purged with argon before the sampling. This minimizes the time flushing the capillaries and the storage loops with reaction gas and allows for a nearly simultaneous (six samples within 60 s) sampling when targeting spatial distribution. The capillaries that connect the reactor with the multiport valve and the pipe connecting the reactor with the pressure control valve are heated to 180 °C to avoid the condensation of water. The water produced by the reaction is collected after the pressure control valve in a condensation flask and the remaining gases are led into the fume hood. Before each experiment, the catalyst is reduced at 400 °C (40 K h^{-1}) for 8 h with a volume flow of H_2 and N_2 of 150 $mL_N min^{-1}$ each.

3 Results

3.1 Catalyst Coating by Screen Printing

Fig. 2a shows an example of the microstructured foils coated with the SPP2080-IMR-catalyst. From the elevation profiles (Fig. 2b) of an empty and a coated microstructured foil, a mean layer thickness of 40 µm can be deduced.

© 2023 The Authors. Chemie Ingenieur Technik published by Wiley-VCH GmbH

15222640, 0, Downloaded from https://onlinelibrary.wiley.com/doi/10.1002/cite.202200204 by Karlsruher Inst F. Technologie, Wiley Online Library on [16/04/2023]. See the Terms and Conditions (https://onlinelibrary.wiley.com/terms-and-conditions) on Wiley Online Library for rules of use; OA articles are governed by the applicable Creative Commons License

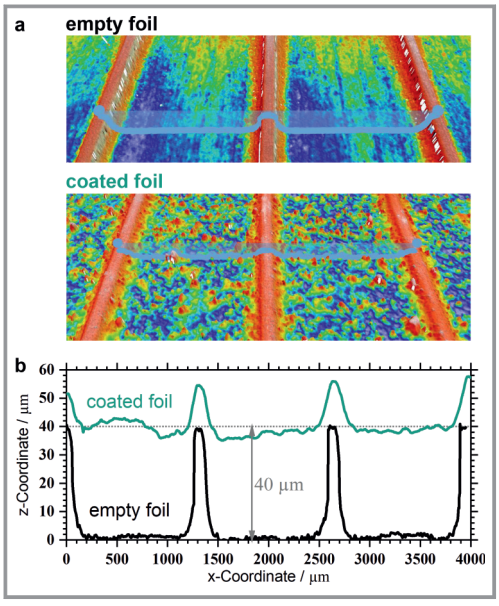

Figure 2. Comparison of the elevation profile of the microstructured foils coated with the SPP2080-IMR catalyst to an empty foil. a) 3D representation and b) exemplary profile of channels, both determined via optical profilometry.

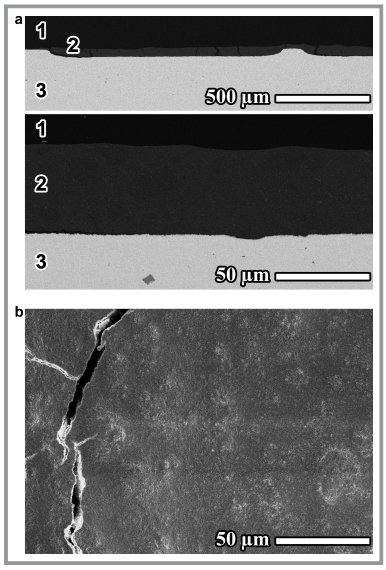

Figure 3. SEM images of the microstructured foils coated with the SPP2080-IMR catalyst. a) Cross-section micrographs, in overview (top) and close-up (bottom). (1) Resin, (2) coated layer, (3) microstructured foil. b) Top-view of the catalyst layer within a channel showing a homogenous catalyst coating and an exemplary crack found in the coating.

This is in accordance with the cross-sectional analysis via scanning electron microscope (SEM, Fig. 3). Both analyses indicate a quite uniform and homogeneous layer thickness distribution. However, SEM and profilometry reveal the occurrence of some larger agglomerates on the layers' surface and some thin layer deposition on the fins between the individual channels. Even though on the macroscopic scale some cracks can be seen in the cross-section scanning electron micrographs, the layers produced show a good adhesion and no peel off is observed (see also Fig. S4). Repeated coatings resulted in a catalyst mass of 18.6 mg ± 4.0 mg per foil measured for 50 foils.

3.2 Temporally Resolved Concentration Profiles at Changing Feed Composition

To demonstrate the feasibility to determine time-resolved concentration profiles at variable feed compositions, the methanation reaction was carried out at T_R = 400 °C, p_R = 5 bar. The feed composition CO_2/H_2 was varied stepwise (1:4 → 1:2 → 1:4 → 1:8 → 1:4) every approx. 5 h *TOS*. In general, 16.7 vol % N_2 was co-fed for dilution and as an internal standard. Volume flow rates of the feed gases including N_2 were adjusted to ensure a constant space velocity of 2.9 $mL_N min^{-1} mg_{cat}^{-1}$ (volume flow corresponds to the total feed gas flow including N_2).

Fig. 4 shows the resulting temporally resolved concentration profiles of CH_4, CO_2, H_2, N_2, and CO measured at the outlet of the reactor. Within the first approx. 5 h, reactants are fed stoichiometrically, immediately resulting in a constant concentration profile with a CO_2 and H_2 conversion of 65.3 and 65.5 %, respectively, and a methane selectivity of 97.4 %. After *TOS* = 5 h, the feed composition was instantly changed from stoichiometric CO_2/H_2 = 1:4 to 1:2. To follow the development of the concentration profile right after the step change in feed composition, time intervals in between the measurements were reduced – the accordant profiles with a temporal resolution of 11 s are also shown in Fig. 4 (bottom). 27 s after the step-change, the CO_2 concentration increases from around 7.5 to 22 % while the H_2 concentration decreases from 28 to 19 %. The concentration of CH_4 decreases slightly from 14 to 12 % and CO increases from 0.5 to 1 % resulting in a lower selectivity to CH_4 after the step change to under-stoichiometric conditions: since now, educts are not anymore fed at stoichiometric ratio, the proportion of CO, which is not further converted to CH_4 increases due to a decrease in the H_2 availability. After 60 s, there is no further change in concentrations observable at the reactor outlet, the reaction now runs again in steady state with a CO_2 and H_2 conversion of 37.9 and 72.4 %, respectively, and a methane selectivity of 92.8 %. After another 6.5 h (*TOS* = 11.5 h), the feed ratio was again changed from CO_2/H_2 = 1:2 back to 1:4 – the accordant profile right after this step in higher temporal resolution is shown in Fig. 4 (bottom). Here, the concentration values approach and finally match the ones of the initial starting point (first set of CO_2/H_2 = 1:4). Constant concentration values are reached again after 60 s with a CO_2 and H_2 conversion of 60.1 and 60.8 %, respectively, and a methane selectivity of 96.2 %. In the next step, H_2 was fed over-stoichiometrically with a ratio of CO_2/H_2 = 1:8. Here, the CO_2 concentration in the product gas decreases from 8.5 to

 © 2023 The Authors. Chemie Ingenieur Technik published by Wiley-VCH GmbH

15222640, 0, Downloaded from https://onlinelibrary.wiley.com/doi/10.1002/cite.202200204 by Karlsruher Inst F. Technologie, Wiley Online Library on [16/04/2023]. See the Terms and Conditions (https://onlinelibrary.wiley.com/terms-and-conditions) on Wiley Online Library for rules of use; OA articles are governed by the applicable Creative Commons License

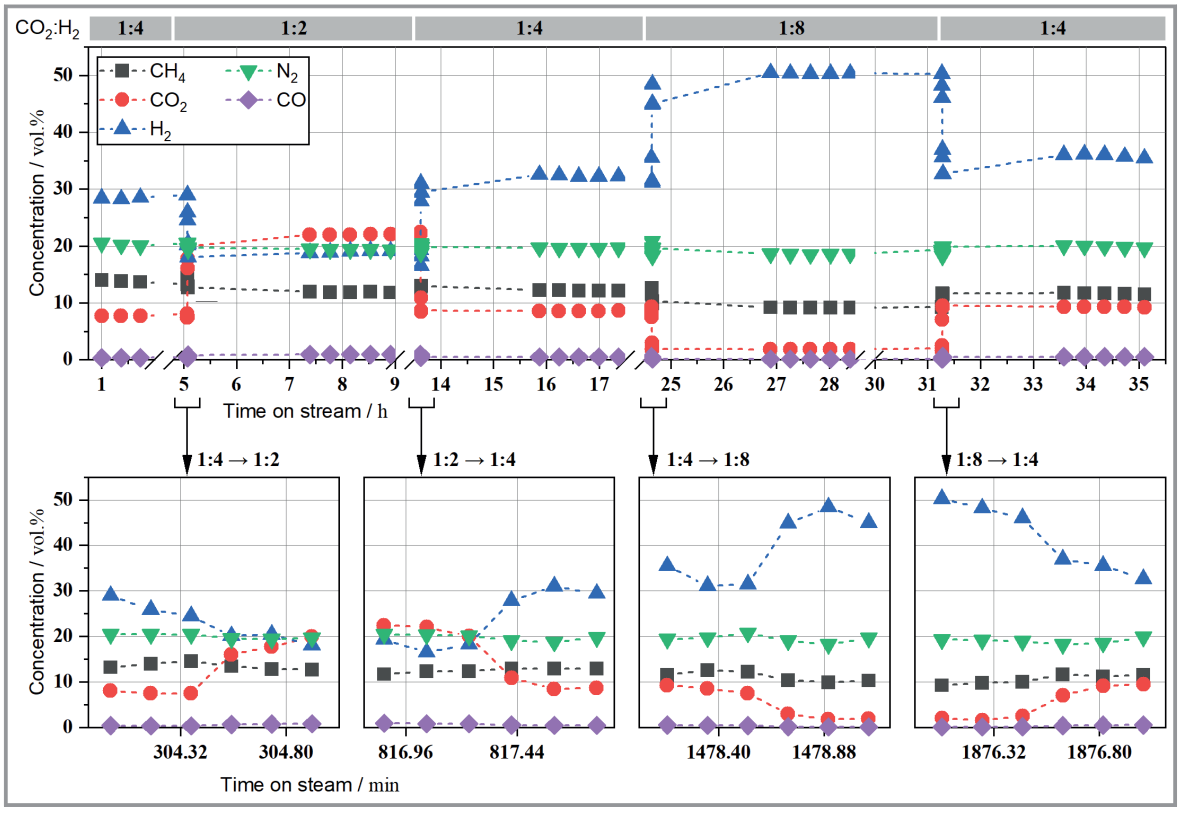

Figure 4. Time-resolved methanation reaction at T_R = 400 °C, p_R = 5 bar, m_{cat} = 103.9 mg, and SV = 2.9 $mL_N min^{-1} mg_{cat}^{-1}$ with varying feed compositions (see indications in graph, in general: 16.7 vol % co-feed of N_2).

1.8 % and the H_2 concentration increases from 32 to 50 %. The concentrations of CH_4 and CO decrease from 12 to 9 % and from 1 to 0.5 %, respectively, when H_2 is fed in excess. Once stationary conditions are reached, a CO_2 and H_2 conversion of 84.0 and 41.7 %, respectively, and a methane selectivity of 98.5 % are achieved. By the last step again stoichiometric conditions were set (CO_2/H_2 = 1:4). As can be seen in Fig. 4, the reactants' concentrations approximately reach again the values of the prior stoichiometric runs. However, over the 35 h time on stream investigated here, a decrease of catalyst activity can be observed (see also Fig. 6). Comparing the initial and final stoichiometric operating point, the conversion of CO_2 and H_2 decreases from 65.3 and 65.5 %, respectively, at 2 h time on stream to 58.1 and 56.4 %, respectively, after 35 h while the methane selectivity also decreases from 97.4 to 95.6 %.

3.3 Spatially Resolved Concentration Profiles at Changing Feed Compositions

The tap reactor presented in this work not only allows for determining concentration profiles at relatively high temporal resolution as outlined in Sect. 3.2, but also for evaluating spatial distribution of the concentration profiles along the reactor coordinate. Fig. 5 shows the CO_2 conversion and CH_4 selectivity profiles at T_R = 400 °C and p_R = 5 bar at the different feed compositions applied in the step experiment (Fig. 4). The spatially resolved profiles shown were recorded right at the end of an accordant set of operation conditions, right before the next set of feed compositions was applied. Not surprisingly, independent of the feed composition investigated, the conversion in general increases along the reactor coordinate, i.e., with the catalyst mass the reactants are in contact with. It is worth mentioning, that for all feed gas compositions the conversion between the last tap and the reactor outlet (dimensionless reactor length of 0.8 and 1.0) stays constant or even decreases, even though the thermodynamic equilibrium is not reached [29]. Since the measurement of the concentration after the reactor is reliable – as the atom balance is fulfilled – and, thus, represents the real gas phase composition, the conversions calculated from the measurements inside the reactor are higher than the actual values. This is due to the fact that the gas sampling via the taps in between the reaction zones is realized at the bottom of the reactor between the catalyst foils (see Sect. 2.1) where the reactants are in direct contact with the catalyst. For the individual taps, a Carberry number of 0.45 or higher was calculated in analogy to [23] which indicates bulk diffusion limitation and, thus, a concentration profile along the height of the reaction channel can be assumed. This eventually results in slightly higher conversion values

© 2023 The Authors. Chemie Ingenieur Technik published by Wiley-VCH GmbH

15222640, 0, Downloaded from https://onlinelibrary.wiley.com/doi/10.1002/cite.202200204 by Karlsruher Inst F. Technologie, Wiley Online Library on [16/04/2023]. See the Terms and Conditions (https://onlinelibrary.wiley.com/terms-and-conditions) on Wiley Online Library for rules of use; OA articles are governed by the applicable Creative Commons License

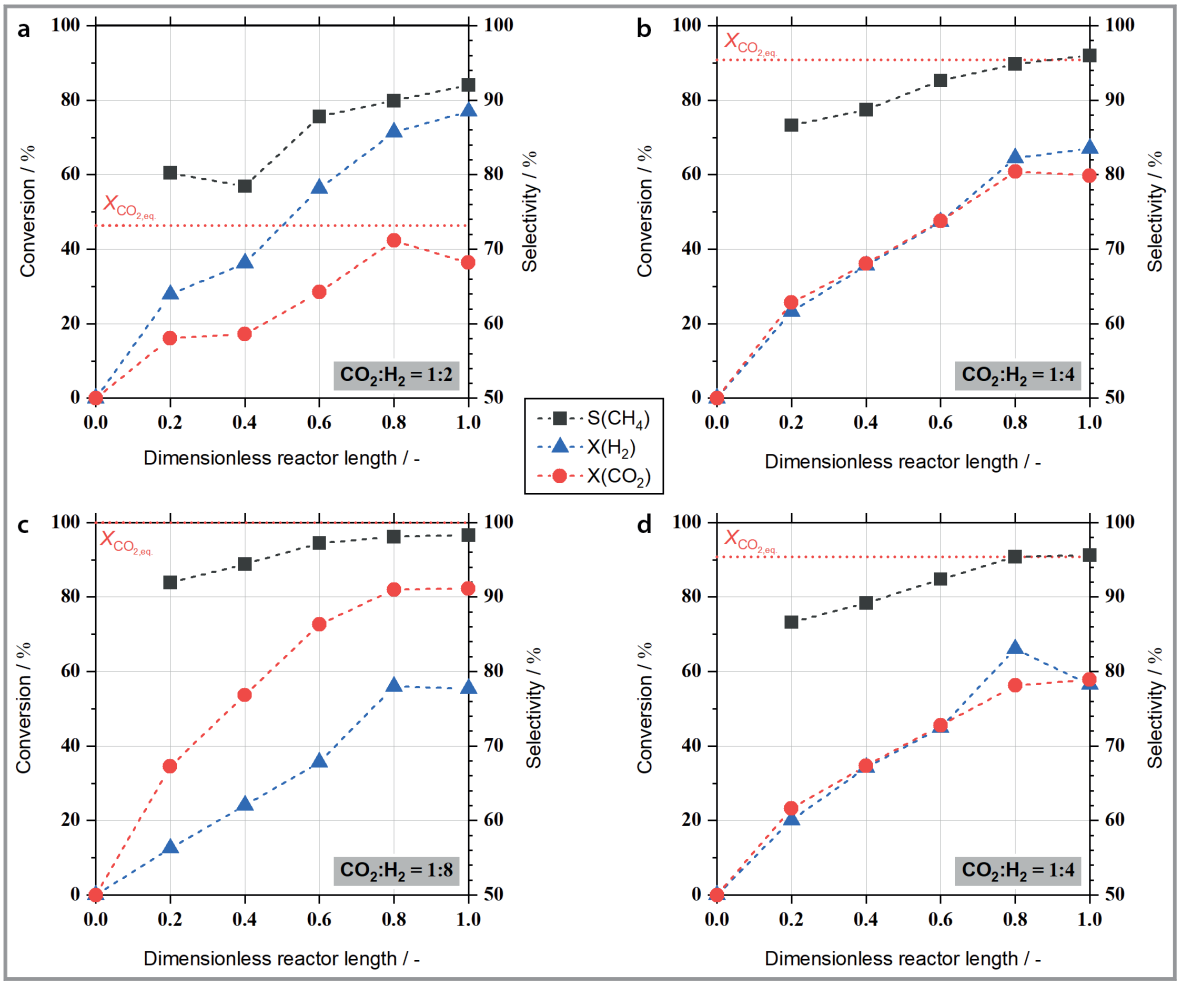

Figure 5. Spatially resolved conversion and selectivity profiles at T_R = 400 °C, p_R = 5 bar, m_{cat} = 103.9 mg, and SV = 2.9 $mL_N min^{-1} mg_{cat}^{-1}$ at varying CO_2/H_2 feed ratio: 1:2 (at TOS = 9 h), 1:4 (at TOS = 17.5 h), 1:8 (at TOS = 29 h), and 1:4 at TOS = 36 h. All samples for each graph were gathered within ΔTOS = 55 s.

of the tap sampling in comparison to the sampling of the outlet downstream of the actual reactor where the gas phase is well mixed. Due to this phenomenon, the conversion values between a dimensionless reactor length of 0.2 and 0.8 are slightly overestimated. Since CO is the only side product with a relevant high concentration and an intermediate product for the methanation reaction, the selectivity increases with the reactor length, i.e., with increasing contacted catalyst mass.

Fig. 5 shows the spatially resolved profiles of the methanation reaction with a variable feed ratio. A ratio of CO_2/H_2 = 1:2 is set at TOS = 9 h. Since the reactants are fed understoichiometrically, the conversion of H_2 is up to 80 % at the end of the reactor, while the conversion of CO_2 is around 40 %. The limitation in H_2 also leads to a lower methane selectivity of 92 % compared to other feed ratios since the CO produced (rWGS) is not fully converted to CH_4. As a side note, the apparent constant values for CO_2 or the decreasing methane selectivity from dimensionless reactor length 0.2 to 0.4 (Fig. 5a) are most likely a result of an unexpected increase in nitrogen concentration (see Fig. S3), which – as the internal standard – mathematically affects the derived metrics. The profiles of the conversions and methane selectivity for a stoichiometric ratio of CO_2/H_2 = 1:4 are shown in Fig. 5 after 17.5 h and 36 h time on stream (individual concentration profiles are shown in Fig. S3). Here, the conversions of CO_2 and H_2 are at similar values due to the stoichiometric feed and a high methane selectivity of around 96 % at the reactor outlet was reached. At the reactor outlet, the conversion of CO_2 reaches 60 % after TOS = 17.5 h and 58 % after TOS = 36 h. Thus, within the 36 h time on stream (cf. Fig. 4), the conversion of CO_2 decreases by 7 % abs. showing the deactivation behavior of the SPP2080-IMR catalyst. The profiles originating from methanation with an overstoichiometric feed ratio of CO_2/H_2 = 1:8 were collected at TOS = 29 h. As H_2 is present in excess, the CO_2 conversion rises to about 82 % and the selectivity of CH_4 reaches over 98 % since methanation of CO (from RWGS) is favored by high H_2 partial pressure.

 © 2023 The Authors. Chemie Ingenieur Technik published by Wiley-VCH GmbH

15222640, 0, Downloaded from https://onlinelibrary.wiley.com/doi/10.1002/cite.202200204 by Karlsruher Inst F. Technologie, Wiley Online Library on [16/04/2023]. See the Terms and Conditions (https://onlinelibrary.wiley.com/terms-and-conditions) on Wiley Online Library for rules of use; OA articles are governed by the applicable Creative Commons License

Further, temperature effects on the methanation reaction were investigated. To exclude conditioning effects by catalyst deactivation of the SPP2080-IMR catalyst, the following pretreatment procedure was applied: for 84 h, the catalyst was exposed to a feed ratio of CO_2/H_2 of 1:8 and 50 vol % dilution with N_2 (m_{cat} = 121.7 mg, SV = 2.5 $mL_N min^{-1} mg_{cat}^{-1}$) at 400 °C and 5 bar. As shown in Fig. 6, within this period of time, the methane selectivity decreased from 99.5 to 98.5 %, the CO_2 and H_2 conversion decreased from 92.4 to 84.8 % and from 49.0 to 43.4 %, respectively, which is comparable to the deactivation during the step changes over 36 h time on stream in Sect. 3.2.

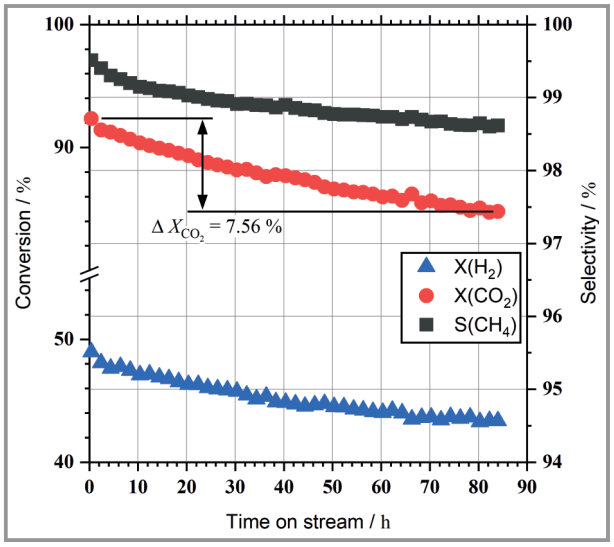

Figure 6. Conversion and selectivity during pretreatment of the SPP2080-IMR catalyst at T_R = 400 °C, p_R = 5 bar, m_{cat} = 121.7 mg, and SV = 2.5 $mL_N min^{-1} mg_{cat}^{-1}$ with overstoichiometric feed (CO_2/H_2 = 1:8), 50 vol % dilution with N_2.

After 84 h time on stream, no significant catalyst deactivation was further observed and, thus, the catalyst could be considered as sufficiently conditioned for the temperature variation experiment.

The spatially resolved analysis (dimensionless reactor length = 0.2–1.0 in steps of 0.2) of the methanation reaction was investigated at five different temperatures (T_R = 300–400 °C in steps of 25 K) at p_R = 5 bar and SV = 4 $mL_N min^{-1} mg_{cat}^{-1}$ with stoichiometric feed (CO_2/H_2 = 1:4), 50 vol % diluted with N_2. Fig. 7 illustrates the heat maps (interpolation between the 5×5 experimental points) for CO_2 and H_2 conversion as well as methane selectivity as a function of dimensionless reactor length and reaction temperature.

The trend of the CO_2 and H_2 conversion follows the expected behavior: with increasing reactor length and increasing temperature the conversion of CO_2 and H_2 increases due to the increasing contacted catalyst mass (reactor length) and a higher reaction rate at higher temperatures since the chemical equilibrium has not been reached. Accordingly, and being in line with the spatially resolved analysis shown above, the methane selectivity reaches the highest value at the end of the reactor at the highest temperature investigated (400 °C).

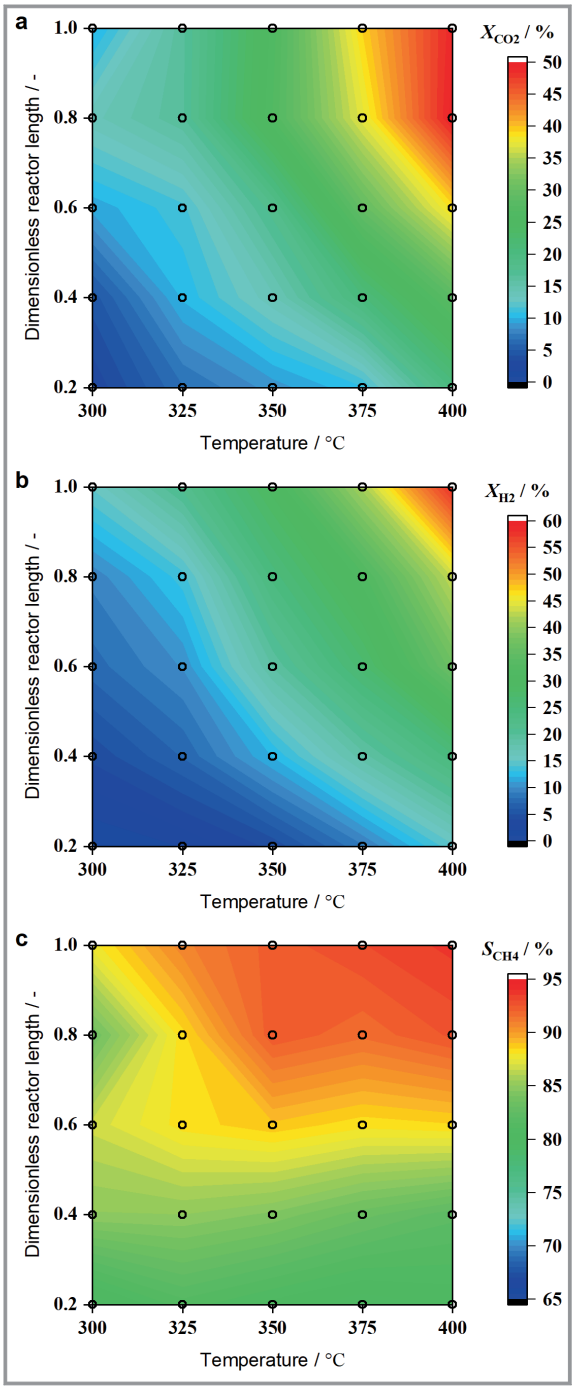

Figure 7. Spatially resolved reaction data as a function of reaction temperature: a) CO_2 conversion, b) H_2 conversion, and c) CH_4 selectivity at p_R = 5 bar and SV = 4 $mL_N min^{-1} mg_{cat}^{-1}$ with stoichiometric feed (CO_2/H_2 = 1:4), 50 vol % diluted with N_2. Heat map shows the interpolation of the 5×5 experimental points indicated by circles.

© 2023 The Authors. Chemie Ingenieur Technik published by Wiley-VCH GmbH

15222640, 0, Downloaded from https://onlinelibrary.wiley.com/doi/10.1002/cite.202200204 by Karlsruher Inst F. Technologie, Wiley Online Library on [16/04/2023]. See the Terms and Conditions (https://onlinelibrary.wiley.com/terms-and-conditions) on Wiley Online Library for rules of use; OA articles are governed by the applicable Creative Commons License

4 Comparison with PFR Model

In a first modeling study, the experimental results from Sect. 3.3 are compared with simulation data. As kinetic expression, a Langmuir-Hinshelwood-Hougen-Watson-type reaction kinetic model, which is developed for describing the IMRC, was used. The model depicts both, the CO_2 methanation and rWGS reaction. Details on the kinetic model structure and its development based on extensive experimental investigations in a complementary kinetic lab scale setup will be discussed in a further upcoming publication. As underlying reactor model, an ideal plug flow reactor (PFR) model is used. The component material balance for each individual reaction zone is expressed in molar form as

$$\frac{\mathrm{d}\dot{n}_i}{\mathrm{d}m_{\mathrm{cat}}} = \sum_{j=1}^{N_{\mathrm{rxn}}} \nu_{i,j} r_j \tag{4}$$

where m_{cat} is the actual catalyst mass which was screen-printed on the accordant microstructured foil placed in the distinct reaction zone, $\dot{n}_i$ is the molar flow rate of component i, r_j is the reaction rate of reaction j, and $\nu_{i,j}$ are the stoichiometric coefficients. To simulate the whole reactor, the material balance is solved for each reaction zone using the corresponding catalyst mass of the individual microstructured foil. As inlet conditions for the first reaction zone the molar flow rates at the reactor inlet are used. The molar flow rates at the end of the upstream reaction zones are used accordingly as inlet conditions for the other reaction zones. The model is implemented and solved in the gPROMS ModelBuilder environment. Each of the five reaction zones is discretized into 25 elements using the built-in first order backward finite differences method (BFDM).

At lower temperatures and conversions, the simulations show already a good match of conversions and selectivity to the measured values (see Fig. 8). With increasing tempera-

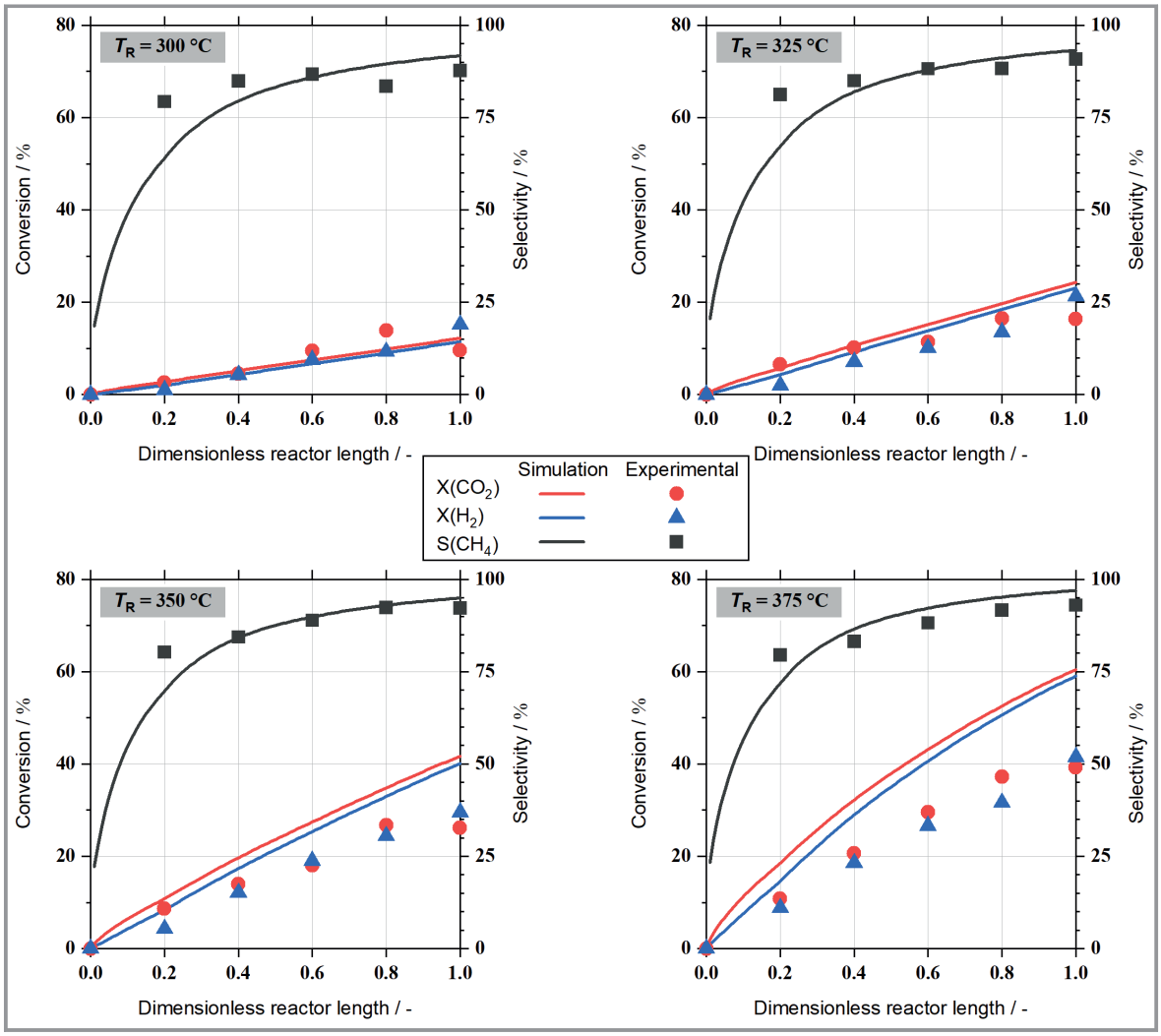

Figure 8. Comparison of experimentally determined spatially resolved conversion and selectivity data versus simulation results of a PFR model at different temperatures. At T_R = variable as indicated, p_R = 5 bar and SV = 4 $mL_N min^{-1} mg_{cat}^{-1}$, m_{cat} = 121.7 mg with stoichiometric feed (CO_2/H_2 = 1:4), 50 vol % diluted with N_2.

 © 2023 The Authors. Chemie Ingenieur Technik published by Wiley-VCH GmbH

15222640, 0, Downloaded from https://onlinelibrary.wiley.com/doi/10.1002/cite.202200204 by Karlsruher Inst F. Technologie, Wiley Online Library on [16/04/2023]. See the Terms and Conditions (https://onlinelibrary.wiley.com/terms-and-conditions) on Wiley Online Library for rules of use; OA articles are governed by the applicable Creative Commons License

ture, however, the deviation between the model prediction and measurements increases due to an overestimation of the conversions in the simulations. This might be caused by a deviating behavior of the tap reactor compared to an ideal PFR. As the gas flows above the catalytic active layer, resistances in mass transport along the channel height and at the phase boundary may occur. These resistances are not considered in the PFR model and can lead to an overestimation of the reaction rates. This conclusion is supported by the observations made in Sect. 3.3, where mass transport phenomena are suspected to falsify the sample collection using the taps along the reactor axis.

For a more precise prediction, more complex reactor models will be necessary. For example, Kopyscinski et al. [22] used successfully one- and two-dimensional heterogeneous reactor models to describe a catalytic plate reactor of similar geometry for the CO methanation reaction. Heterogeneous models depict the mass transport at gas phase-catalyst boundary. Two-dimensional models are able to describe gradients along the flow channel height. Both of these effects can become relevant, depending on the characteristics of the reactor set up and the operating conditions. Nevertheless, the results of the PFR simulations serve for the purpose of this study, which is the validation of the newly designed tap reactor system along with the analytics.

5 Summary and Conclusion

In this contribution, a tap reactor is presented allowing for sampling the gas phase at four taps along the reactor coordinate. The applied analytic set up further allows for temporally resolved measurements at a resolution of 11 s. In particular, the tap reactor was applied to study the CO_2 methanation reaction over a Ni-based IMRC which was coated via screen printing on five microstructured foils integrated into five reaction zones within the tap reactor. A reproducible and homogenous layer of the Ni catalyst with a layer thickness of approx. 40 µm and good adhesion was achieved. Experiments with transient operating conditions (changing feed composition CO_2/H_2 = 1:2, 1:4, 1:8) were carried out. Besides the changes in selectivity and conversion, which are to be expected, a decrease of catalyst activity over time was found due to deactivation. Additionally, conversion and selectivity profiles along the reactor coordinate as a function of reaction temperature (T_R = 300–375 °C) were measured and compared to PFR simulations using a kinetic model developed for the IMRC. Especially at the higher reaction temperatures, the simulations overestimate the conversion compared to the measurements. This can be attributed to differences in the flow profile, which will be investigated in more detail in future studies. However, the comparison validates the approach applied. Further, the tap reactor is designed in a way that the cover lid can be replaced by a ZnS window – in upcoming studies diffuse reflectance infrared spectroscopy (DRIFTS) will be used to likewise obtain spatially resolved operando spectra. In combination with the spatially and temporally resolved gas phase analytics presented in this work, the DRIFTS measurements will provide additional information to investigate the dynamics and the deactivation behavior of methanation catalysts.

Supporting Information

Supporting Information for this article can be found under DOI: https://doi.org/10.1002/cite.202200204.

Acknowledgment

The authors would like to acknowledge funding by the German Research Foundation (DFG priority program 2080 "Catalysts and reactors under dynamic conditions for energy storage and conversion", Grant No. KL 3223/1-2 and FR 2918/3-2). The authors also would like to thank Barbara Berzl and Georg Rabsch for their support and effort in designing the tap reactor. Open access funding enabled and organized by Projekt DEAL.

Symbols used

ΔH_R^0	[kJ mol^{-1}]	reaction enthalpy at standard conditions
m_{cat}	[g]	catalyst mass
$\dot{n}_i$	[mol s^{-1}]	molar flow rate of component i
p_R	[bar(a)]	reaction pressure
r_j	[mol $g_{cat}^{-1} s^{-1}$]	reaction rate of reaction j
SV	[$mL_N min^{-1} mg_{cat}^{-1}$]	space velocity ($mL_N min^{-1}$ of total gas flow including N_2)
TOS	[h]	time on stream
T_R	[°C]	reaction temperature
$\nu_{i,j}$	[–]	stoichiometric coefficient of component i in reaction j

Abbreviations

BFDM	backward finite differences method
DRIFTS	diffuse reflectance infrared fourier transform spectroscopy
IMRC	industrial methanation rreference catalyst
PFR	plug-flow reactor
PtX	power-to-X
rWGS	reverse water-gas shift
RZ	reaction zone
SEM	scanning electron microscope

© 2023 The Authors. Chemie Ingenieur Technik published by Wiley-VCH GmbH

15222640, 0, Downloaded from https://onlinelibrary.wiley.com/doi/10.1002/cite.202200204 by Karlsruher Inst F. Technologie, Wiley Online Library on [16/04/2023]. See the Terms and Conditions (https://onlinelibrary.wiley.com/terms-and-conditions) on Wiley Online Library for rules of use; OA articles are governed by the applicable Creative Commons License

References

[1] A. Ari, N. Arregui, S. Black, O. Celasun, D. Iakova, A. Mineshima, V. Mylonas, I. Parry, I. Teodoru, K. Zhunussova, *Surging Energy Prices in Europe in the Aftermath of the War: How to Support the Vulnerable and Speed up the Transition Away from Fossil Fuels*, IMF Working Paper, WP/22/152, International Monetary Fund, Washington, D.C. **2022**.

[2] P. Sabatier, J. B. Senderens, *C. R. Acad. Sci.* **1902**, *134*, 514–516.

[3] P. Sabatier, J. B. Senderens, *C. R. Acad. Sci.* **1902**, *134*, 689–691.

[4] E. Baraj, S. Vagaský, T. Hlinčik, K. Ciahotný, V. Tekáč, *Chem. Pap.* **2016**, *70 (4)*, 395–403. DOI: https://doi.org/10.1515/chempap-2015-0216

[5] K. F. Kalz, R. Kraehnert, M. Dvoyashkin, R. Dittmeyer, R. Gläser, U. Krewer, K. Reuter, J.-D. Grunwaldt, *ChemCatChem* **2017**, *9 (1)*, 17–29. DOI: https://doi.org/10.1002/cctc.201600996

[6] M. Marwood, R. Doepper, M. Prairie, A. Renken, *Chem. Eng. Sci.* **1994**, *49 (24A)*, 4801–4809. DOI: https://doi.org/10.1016/S0009-2509(05)80060-0

[7] M. Marwood, F. van Vyve, R. Doepper, A. Renken, *Catal. Today* **1994**, *20*, 437–448. DOI: https://doi.org/10.1016/0920-5861(94)80137-1

[8] D. Meyer, J. Friedland, J. Schumacher, R. Güttel, *Chem. Eng. Res. Des.* **2021**, *173*, 253–266. DOI: https://doi.org/10.1016/j.cherd.2021.07.011

[9] B. Kreitz, J. Friedland, R. Güttel, G. D. Wehinger, T. Turek, *Chem. Ing. Tech.* **2019**, *91 (5)*, 576–582. DOI: https://doi.org/10.1002/cite.201800191

[10] S. Theurich, S. Rönsch, R. Güttel, *Energy Technol.* **2020**, *8 (3)*, 1901116. DOI: https://doi.org/10.1002/ente.201901116

[11] B. Mutz, H. W. P. Carvalho, S. Mangold, W. Kleist, J.-D. Grunwaldt, *J. Catal.* **2015**, *327*, 48–53. DOI: https://doi.org/10.1016/j.jcat.2015.04.006

[12] B. Mutz, A. Gänzler, M. Nachtegaal, O. Müller, R. Frahm, W. Kleist, J.-D. Grunwaldt, *Catalysts* **2017**, *7 (9)*, 279. DOI: https://doi.org/10.3390/catal7090279

[13] J.-S. Choi, W. P. Partridge, C. S. Daw, *Appl. Catal., A* **2005**, *293*, 24–40. DOI: https://doi.org/10.1016/j.apcata.2005.06.025

[14] J.-S. Choi, W. P. Partridge, J. A. Pihl, M.-Y. Kim, P. Kočí, C. S. Daw, *Catal. Today* **2012**, *184 (1)*, 20–26. DOI: https://doi.org/10.1016/j.cattod.2011.11.007

[15] M. Eck, P. Lott, D. Schweigert, M. Börnhorst, O. Deutschmann, *Chem. Ing. Tech.* **2022**, *94 (5)*, 738–746. DOI: https://doi.org/10.1002/cite.202100192

[16] J. Sá, D. L. A. Fernandes, F. Aiouache, A. Goguet, C. Hardacre, D. Lundie, W. Naeem, W. P. Partridge, C. Stere, *Analyst* **2010**, *135 (9)*, 2260–2272. DOI: https://doi.org/10.1039/c0an00303d

[17] O. Shakir, A. Yezerets, N. W. Currier, W. S. Epling, *Appl. Catal., A* **2009**, *365 (2)*, 301–308. DOI: https://doi.org/10.1016/j.apcata.2009.06.033

[18] R. Horn, K. A. Williams, N. J. Degenstein, L. D. Schmidt, *Chem. Eng. Sci.* **2007**, *62 (5)*, 1298–1307. DOI: https://doi.org/10.1016/j.ces.2006.11.030

[19] R. Horn, K. A. Williams, N. J. Degenstein, A. Bitschlarsen, D. Dallenogare, S. Tupy, L. Schmidt, *J. Catal.* **2007**, *249 (2)*, 380–393. DOI: https://doi.org/10.1016/j.jcat.2007.05.011

[20] R. Horn, N. J. Degenstein, K. A. Williams, L. D. Schmidt, *Catal. Lett.* **2006**, *110 (3–4)*, 169–178. DOI: https://doi.org/10.1007/s10562-006-0117-8

[21] M. Bosco, F. Vogel, *Catal. Today* **2006**, *116 (3)*, 348–353. DOI: https://doi.org/10.1016/j.cattod.2006.05.064

[22] J. Kopyscinski, T. J. Schildhauer, F. Vogel, S. M. A. Biollaz, A. Wokaun, *J. Catal.* **2010**, *271 (2)*, 262–279. DOI: https://doi.org/10.1016/j.jcat.2010.02.008

[23] J. A. Hernandez Lalinde, K. Kofler, X. Huang, J. Kopyscinski, *Catalysts* **2018**, *8 (2)*, 86. DOI: https://doi.org/10.3390/catal8020086

[24] J. A. Hernandez Lalinde, P. Roongruangsree, J. Ilsemann, M. Bäumer, J. Kopyscinski, *Chem. Eng. J.* **2020**, *390*, 124629. DOI: https://doi.org/10.1016/j.cej.2020.124629

[25] V. Surendran, M. Bracconi, J. A. Hernandez Lalinde, M. Maestri, J. Kopyscinski, *Chem. Eng. J.* **2022**, *446*, 136999. DOI: https://doi.org/10.1016/j.cej.2022.136999

[26] S. Weber, K. L. Abel, R. T. Zimmermann, X. Huang, J. Bremer, L. K. Rihko-Struckmann, D. Batey, S. Cipiccia, J. Titus, D. Poppitz, C. Kübel, K. Sundmacher, R. Gläser, T. L. Sheppard, *Catalysts* **2020**, *10 (12)*, 1471. DOI: https://doi.org/10.3390/catal10121471

[27] S. Weber, R. T. Zimmermann, J. Bremer, K. L. Abel, D. Poppitz, N. Prinz, J. Ilsemann, S. Wendholt, Q. Yang, R. Pashminehazar, F. Monaco, P. Cloetens, X. Huang, C. Kübel, E. Kondratenko, M. Bauer, M. Bäumer, M. Zobel, R. Gläser, K. Sundmacher, T. L. Sheppard, *ChemCatChem* **2022**, *14*, e202101878. DOI: https://doi.org/10.1002/cctc.202101878

[28] D. Weber, K. M. Wadlinger, M. M. Heinlein, T. Franken, *ChemCatChem* **2022**, *14*, e202200563. DOI: https://doi.org/10.1002/cctc.202200563

[29] K. Ghaib, K. Nitz, F.-Z. Ben-Fares, *ChemBioEng Rev.* **2016**, *3 (6)*, 266–275. DOI: https://doi.org/10.1002/cben.201600022

 © 2023 The Authors. Chemie Ingenieur Technik published by Wiley-VCH GmbH

15222640, 0, Downloaded from https://onlinelibrary.wiley.com/doi/10.1002/cite.202200204 by Karlsruher Inst F. Technologie, Wiley Online Library on [16/04/2023]. See the Terms and Conditions (https://onlinelibrary.wiley.com/terms-and-conditions) on Wiley Online Library for rules of use; OA articles are governed by the applicable Creative Commons License

DOI: 10.1002/cite.202200204

Tap Reactor for Temporally and Spatially Resolved Analysis of the CO_2 Methanation Reaction

Timo Engl, Moritz Langer, Hannsjörg Freund, Michael Rubin, Roland Dittmeyer*

Research Article: This research article presents a tap reactor for in-depth investigations of the CO_2 methanation reaction over a catalyst implemented as coating. Spatially and temporally resolved reaction data under various operating conditions including transient operation are discussed. A comparison with simulation data validates the presented approach.

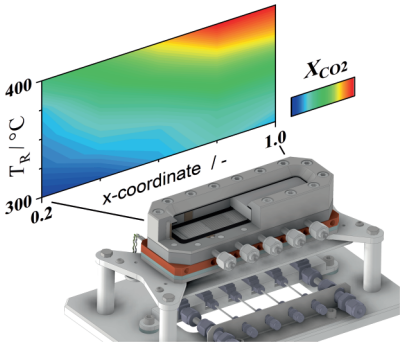

Supporting Information available online

© 2023 The Authors. Chemie Ingenieur Technik published by Wiley-VCH GmbH

15222640, 0, Downloaded from https://onlinelibrary.wiley.com/doi/10.1002/cite.202200204 by Karlsruher Inst F. Technologie, Wiley Online Library on [16/04/2023]. See the Terms and Conditions (https://onlinelibrary.wiley.com/terms-and-conditions) on Wiley Online Library for rules of use; OA articles are governed by the applicable Creative Commons License